**Can land surface models capture the observed soil moisture control of water and carbon fluxes in temperate-to-boreal forests?**

T. dos Santos, G. Keppel-Aleks, R. De Roo, A.L. Steiner[1]

Department of Climate and Space Sciences and Engineering
University of Michigan, Ann Arbor
Ann Arbor, MI 48109-2143

[1] Corresponding Author:  Allison L. Steiner, alsteine@umich.edu

**Key points**
- CLM latent heat flux biases at deciduous sites are related to soil moisture biases, and capture the observed seasonal cycle and soil moisture relationships
- CLM modeled GPP is underestimated compared to Fluxnet and SMAP L4 data and is uncoupled from latent heat seasonal changes
- Individual environmental variables (temperature, radiation, soil moisture) do not provide a mechanistic explanation of site-to-site variability, suggesting complex canopy processes

**Abstract**

The reservoir of soil water is exchanged with the atmosphere through evaporative processes, which are mediated via vegetation through transpiration.  Carbon uptake is closely coupled to transpiration, and most process-based models link transpiration and photosynthesis explicitly.  Here we evaluate the simulation of water and carbon fluxes in forested areas of North America using point-based simulations of the Community Land Model version 5 (CLM5) with Soil Moisture Active/Passive (SMAP) satellite derived soil moisture measurements and in situ measurements at eight Fluxnet and two United States Climate Research Network (CRN) sites.  Compared to observations, there is a broad site-to-site variability in simulated soil moisture, with some sites exhibiting wet biases and others dry biases.  The bias sign does not depend on ecosystem or other environmental drivers such as radiation and temperature.  Compared to Fluxnet latent heat (LH) and gross primary production (GPP) flux tower observations, simulated LH flux biases at deciduous broadleaf forests are linked with soil moisture biases, and the model captures the observed seasonal cycle and parabolic seasonal relationship with soil moisture.  The parabolic shape is driven by high soil moisture and low LH fluxes in June, peak LH and drier soil conditions

in July, followed by further soil moisture drawdown in August. GPP is underestimated at most sites, and the model exhibits a linear relationship between soil moisture and GPP. Because the photosynthesis parameterizations are similar in most Earth system models, further model development that incorporates observations and observed relationships is needed to accurately capture the GPP-soil moisture relationship.

**Index Terms**

0416:  Biogeophysics

0426 Biosphere-atmosphere interactions

0428 Carbon cycle

3322 Land-atmosphere interactions

1813 Ecohydrology

1878 Water/energy cycles

## 1. Introduction

Soil moisture acts as a key driver in the climate system by controlling water and carbon exchange between the surface and the atmosphere [*Seneviratne et al.*, 2010]. In vegetated regions, this relationship becomes more complex because vegetation relies on water from its rooting system. As a result, the amount of soil moisture present controls the photosynthetic and evaporative demand of vegetated regions. While other environmental drivers such as temperature and precipitation are often used to explain the exchange of water and carbon, the role of soil moisture and its limiting effect on ecosystem functioning is possibly more fundamental but still very poorly constrained. Therefore, understanding soil moisture-water-carbon interactions is key to understanding regional hydroclimatology and precipitation [*Dirmeyer et al.*, 2009; *Seneviratne et al.*, 2010], as well as understanding the regional and global projections of the terrestrial carbon [*Suyker et al.*, 2003].

Terrestrial vegetation mobilizes moisture from the subsurface to the non-woody parts of the plant (e.g., stems and leaves) through its rooting system. Green biomass converts radiant energy to chemical energy through photosynthesis, the process that converts carbon dioxide ($CO_2$) into carbohydrates and new biomass. To draw $CO_2$ from the atmosphere into the leaf for fixation, leaves have openings on their surface known as stomates. When the stomates open to allow $CO_2$ into the leaf, water vapor inexorably escapes due to the strong gradient from the nearly saturated environment inside the leaf to the relatively dry atmosphere. This biological process of stomatal control inherently couples the water and carbon cycle when vegetation is present, and it is difficult to examine carbon exchange without understanding the relative role of evapotranspiration and the limitations of soil moisture.

In vegetated regions, evapotranspiration (ET) is the sum of evaporation from the ground, evaporation from water stored within the canopy, and transpiration or the release of water from the internal plant tissues during stomatal opening. Ground-based observations from flux towers [*Baldocchi and Wilson*, 2001] and satellite-derived ET [*Mu et al.*, 2011] both estimate total evapotranspiration from ecosystems. However, models still show difficulty

3

in accurately simulating ET in vegetated regions over a range of time scales from daily [*Matheny et al.*, 2014] to interannual [*Jung et al.*, 2010]. To understand the role of soil moisture on modeled ET, observationally based metrics indicate that ET is still underestimated by models, particularly during the summer months when soil moisture may not be properly represented. For example, NLDAS experiments show that even with data assimilation techniques, models still underestimate summer ET [*Xia et al.*, 2015].

Because of the tight coupling of transpiration with carbon, soil moisture also has the potential to influence global gross primary productivity (GPP, or the net carbon assimilated during photosynthesis) on a range of time scales (e.g. [*Lei et al.*, 2014]. Global scale simulations suggest that moisture stress in temperate Northern Hemisphere ecosystems is an important driver of interannual variability of carbon sinks [*Keppel-Aleks et al.*, 2014], and the precipitation-productivity relationship is likely derived through vegetation uptake of soil water. The impact of climate stress on Northern Hemisphere ecosystems is substantial: the coupled influences of temperature and drought stress, as measured by Palmer Drought Severity Index, in the Northern Hemisphere mid- to high-latitudes contribute 0.23 Pg C $y^{-1}$ variability to the global carbon sink (or about 10% of the average annual sink). The covariance of temperature and drought stress in their relationship to net carbon fluxes indicate that soil moisture may affect the temperature anomaly over land via latent heat and the surface energy balance.

While most studies suggest that soil moisture is a strong driver in water and carbon exchange, the lack of broad scale soil moisture observations has precluded clear observable metrics to quantify soil moisture's role. Large-scale modeling studies can simulate very different amounts of soil water yet similar temporal patterns on the seasonal scale [*Koster et al.*, 2009], suggesting that modeled soil moisture is still poorly constrained. Frequently, the role of soil moisture as a driver has been explained in the energy-limited vs. moisture-limited framework (e.g., as reviewed in [*Seneviratne et al.*, 2010]), yet clearly defining the soil moisture limitations is still needed to understand the role of soil moisture limitations on water and carbon fluxes. In January 2015, NASA launched the Soil Moisture Active Passive (SMAP) satellite, developed to address the lack of soil moisture data at broad

4

spatial scales [*Entekhabi et al.*, 2014], providing a unique opportunity to understand surface soil moisture at broad spatial scales.

Forested areas are difficult regions for understanding the role of soil moisture, yet they represent one of the most important ecosystem types to understand because of their high throughput of carbon and water. Challenges in understanding soil moisture in these regions include (1) the density of vegetation, which complicates remote-sensing techniques retrievals, (2) the complexity of the root structure, with different types of vegetation contributing different root zones, and (3) the heterogeneity of the rooting systems and subsequent soil moisture. In this paper, we focus on the temperate to boreal transition region over North America (approximately 40-65°N). Temperate forests are a mix of deciduous broadleaf and evergreen needleleaf trees, and can be classified using plant functional type (PFT) categorizations as deciduous broadleaf forests (DBF), evergreen needleleaf forests (ENF), or mixed forest. Boreal forests represent the regions across Eurasia and Northern America just south of the tundra line, and they can be ENF, or in some cases, DBF. These two dominant PFTs in the temperate-to-boreal transition zone have different surface energy budgets and utilization of water, which likely affects the soil moisture relationship to water and energy fluxes.

In this manuscript, we aim to (1) evaluate simulations of soil moisture using a widely used land model, the Community Land Model version 5 (CLM5; [*Lawrence et al.*, 2019]) with both in situ and remotely sensed soil moisture from the NASA SMAP satellite retrievals and (2) understand and quantify soil moisture controls on water and carbon fluxes in the temperate to boreal transition region of North America, where we have a substantial number of in situ measurements.

## 2. Observational datasets
### 2.1. SMAP soil moisture observations

5

SMAP is the latest L-band NASA satellite mission that provides soil moisture in the top 5 cm of the soil at the global scale [*Entekhabi et al.*, 2014]. The SMAP radiometer observes the Earth's surface with a near-polar, Sun-synchronous 6:00 a.m. (descending)/6:00 p.m. (ascending) orbit. In this study, we use SMAP radiometer estimates derived from the observations acquired from the 6:00 a.m. (local time) descending passes as they have been found to be relatively more accurate than the 6:00 p.m. passes (Chan et al., 2018).

We use the SMAP Enhanced Level 3 Radiometer Global Daily 9 km EASE-GRID [*O'Neill et al.*, 2018]passive soil moisture product (L3SMPE) with data coverage from 1 April 2015–31 Nov 2018 to evaluate model simulations over the study area. The L3SMPE product is a daily gridded global composite based on the half-orbit SMAP Level 2 soil moisture product (L2SMP), where the retrieval can be is summarized as follows: 1) the surface brightness temperature observed by the SMAP radiometer is converted to surface emissivity; 2) surface emissivity is corrected by removing the effects of vegetation; 3) surface emissivity is further corrected by accounting for the effects of the soil surface roughness; 4) the Fresnel equation is used to relate soil emissivity and soil permittivity; 5) the Mironov dielectric mixing model is used to convert the dieletric properties to soil moisture.  We also include the SMAP Level 4 (L4) daily global primary productivity (GPP) and 3-hourly surface soil moisture data at 9 km resolution for comparison with model simulations and ground-based observations from the Fluxnet network.  The L4 product for soil moisture merges SMAP surface soil moisture estimates with the Catchment model for vertical moisture transport within the soil column and GPP estimates [*Reichle et al.*, 2017].  The L4 GPP is then derived from a data-driven terrestrial ecosystem model that uses MODIS fPAR and vegetation data together with SMAP L4 soil moisture [*Jones et al.*, 2017].

SMAP observations are reported on the EASE grid as percentage of soil volumetric water content.  Although full spatial coverage is provided, data in regions where the vegetation canopy water content exceeded 5 kg m$^{-2}$ are considered unreliable [*Das et al.*, 2011; *Entekhabi et al.*, 2010].  These restrictions on the data in forested regions required the utilization of other in situ soil moisture observations, as described below.

6

## 2.2. Fluxnet surface observations

The Fluxnet network (https://fluxnet.fluxdata.org/) provides observations of ecosystem carbon, water, and energy (sensible and latent heat) fluxes at sites across the globe. Fluxnet tower locations also provide measurements of climate variables, including air temperature, relative humidity and soil moisture at half-hourly or hourly temporal resolutions. In this study, we focused on analysis of soil moisture, latent heat, and GPP fluxes, but also meteorological data from the towers for model forcing. We therefore selected Fluxnet sites in the North American temperate-to-boreal transition zone based on three criteria, including (1) land cover classified as evergreen needleleaf forest (ENF) and deciduous broadleaf forest (DBF), (2) availability of both model forcing (downward short- and long-wave radiation, precipitation, air temperature and wind speed) and evaluation (latent heat, GPP) variables to drive point-based CLM simulations and (3) are within the 35-64°N and 70-110°W forested region in North America, encompassing the central US temperate to boreal transition zone. A total of 8 sites met these criteria (Table 1). Because they span different time periods, our analysis focuses on the 2004-2010 time period, which all sites have in common.

We analyzed gap-filled observations of latent heat fluxes and GPP. We note that GPP is not observed directly using eddy covariance, but is inferred from net ecosystem exchange observations after making assumptions about ecosystem respiration. We used the GPP estimated from the daytime partitioning method [*Lasslop et al.*, 2010] from the tower sites. The gap-filled tower fluxes and meteorology data were available at either 30- or 60-minute frequency, depending on site. Soil moisture observations were only consistently available at a surface layer (5 cm) across the selected sites, which corresponds to the surface layer of the model simulations.

## 2.3. United States Climate Reference Network (USCRN)

The United States Climate Reference Network (USCRN) is maintained by the National Climatic Data Center (NCDC) and collects in situ measurements of soil moisture at 114 sites

7

nationwide. USCRN soil moisture data are available at

http://www1.ncdc.noaa.gov/pub/data/uscrn/products/soilsip01/. Each station consists of soil moisture sensors placed at 5, 10, 20, 50, and 100 cm depths [*Bell et al.*, 2013]. Given the restrictions on VWC from SMAP, our study was limited to two sites: Shabonna, IL and Goodridge, MN, where we use hourly observations of soil moisture at 5 cm depth.

## 3.0 CLM5 Model description

We use version 5 of the CLM (CLM5;[*Lawrence et al.*, 2019]), which is the land component of the Community Earth System Model (CESM). CLM5 simulates the exchange of mass and energy between the atmosphere to the land surface. The biogeophysical processes represented in CLM include the surface energy budget, accounting for solar and longwave radiation fluxes, turbulent energy fluxes from canopy and soil, and heat transfer in soil and snow.

CLM5 also simulates the hydrology of both soil and canopy, which is controlled by stomatal physiology and linked to vegetation photosynthesis. Here we focus on describing CLM's approach to simulating soil and plant hydraulics, a key aspect of this study. For a full description of the CLM model, the reader is referred to [*Oleson et al.*, 2013] (CLM4.5) and [*Lawrence et al.*, 2019] (CLM5). Within the soil, CLM5 uses Darcy's law to describe the vertical flux of water, which depends on the hydraulic conductivity of the soil column and is a function of soil texture (i.e. fractions of sand, silt and clay) and root water uptake.  For transpiration, stomatal conductance regulates the exchange of water and carbon between the atmosphere and the vegetation canopy. Vegetation must optimize between carbon uptake and water loss through stomata, and thus stomatal conductance is affected by soil water stress. At the climate time scale, [*Bryan et al.*, 2015] shows that the Community Land Model (CLM) under predicts the observed temperature-evapotranspiration relationship in mid-latitude deciduous forests, which may be related to erroneous soil water content or poorly parameterized transpiration processes.  Here, we analyze two different model parameterizations that account for the coupling between stomatal conductance and soil

8

moisture stress, described below, to understand the impacts of soil moisture on surface fluxes.

### 3.1 Ball-Berry model with soil moisture stress (CLM5-SMS)

The Ball-Berry model [*Ball et al.*, 1987] describes stomatal conductance ($g_s$) based on empirical relationships between net photosynthesis ($A_n$), relative humidity ($H_s$), $CO_2$ concentration ($c_s$) at the leaf surface, minimum stomatal conductance ($g_o$, when $A_n$ approaches zero), and an empirical slope constant $g_1$:

$$g_s = g_0 + g_1 \left( \frac{A_n H_s}{c_s} \right) \tag{1}$$

Net photosynthesis is calculated based on [*Farquhar et al.*, 1980], wherein the photosynthesis rate is determined by colimitation among the Rubisco-, light-, and export-limited rates [*Bonan et al.*, 2011]. The Rubisco-limited rate depends on the maximum rate of carboxylation, $V_{cmax}$, which can also be affected by model biogeochemistry (see Section 3.3). The value for $g_1$ is prescribed based on plant functional type (4.45 for DBF and 2.35 for ENF) and does not vary between boreal and temperate ecosystems.

The soil moisture stress function (hereafter referred to as CLM5-SMS) uses a parameter $\beta$ defined as:

$$\beta = 0 \leq \frac{\psi_c - \psi_s}{\psi_c - 0} \leq 1 \tag{2}$$

where $\psi_c$ is the soil water potential (i.e., suction force) at which stomata close, $\psi_o$ is the soil water potential when the stomata are fully open, and $\psi_s$ is the soil water potential at the current model timestep. The parameters $\psi_c$ and $\psi_o$ are assigned based on predawn leaf water potential measurements [*White et al.*, 2000] and have values of -2.55 and -0.66 MPa respectively for temperate and boreal evergreen needleleaf trees and -2.24 and -0.35 MPa respectively for temperate and boreal deciduous broadleaf trees [*Oleson et al.*, 2013]. In CLM, the soil moisture stress function $\beta$ of Equation (2) can influence $g_s$ (Equation 1) by directly multiplying $\beta$ and $g_o$. The value of $\beta$ is also prescribed by plant functional type, and does vary for temperate and boreal ecosystems, with a value of 0.976 for ENF temperate, 0.966 for DBF temperate, and 0.943 for both DBF and ENF boreal.

9

### 3.2 Medlyn Stomatal Conductance with Plant Hydraulic Stress (CLM5-PHS)

In CLM5, the Ball-Berry model was replaced with the Medlyn conductance model [*Medlyn et al.*, 2011] because of its more realistic behavior at low humidity levels [*Rogers et al.*, 2017]. Similar to Ball-Berry, the Medlyn model is based on the leaf gas exchange equation but it uses vapor pressure deficit near the leaf surface ($D_s$) instead of relative humidity:

$$g_s = g_0 + 1.6 \left(1 + \frac{g_1}{\sqrt{D_s}}\right)\frac{A_n}{c_s} \qquad (3)$$

Likewise, the slope parameter can vary according to plant functional types in the Medlyn formulation (see values under the Ball-Berry/CLM5-SMS description above).

CLM5 also introduces a more sophisticated approach to calculate soil moisture stress known as plant hydraulic stress (PHS; Kennedy et al., 2019), which solves for the water potential of roots, stems and leaves. Water transpiration through the stomata must be balanced at every model timestep by flow through the roots and stems, where the root uptake of water is parameterized. The impact of soil moisture stress on transpiration, and ultimately net photosynthesis, is thus modeled by ensuring that leaf water potential does not fall below a critical threshold. [*Franks et al.*, 2018] notes that the Medlyn and Ball-Berry stomatal conductance parameters can be adjusted to achieve similar water and carbon fluxes between the two models, and while we do not explicitly test these two stomatal parameterizations individually here, [*Wozniak et al.*, 2020] found that for canopy-scale water and carbon fluxes, the hydraulic strategy (e.g., SMS vs. PHS) had a greater influence on water and carbon fluxes than the stomatal conductance parameterization. Based on these two studies, we expect that the model differences between CLM5-SMS and CLM5-PHS are largely driven by the soil moisture limitations.

### 3.3 Biogeochemistry in CLM5

In addition to biogeophysics, CLM5 also simulates carbon-nitrogen biogeochemistry (BGC) [*Thornton et al.*, 2007]. Of relevance to the analysis here which focuses only on carbon fluxes due to GPP, nitrogen availability can downregulate photosynthesis in the model. CLM5 includes updated parameterizations to account for nitrogen limitation, one of

10

which permits flexible ratios of carbon to nitrogen within leaves rather than having a static value and thereby avoids instantaneous down-regulation of photosynthesis [*Lawrence et al.*, 2019]. Likewise, the BGC parameterization in CLM5 allows for the maximum rate of carboxylation to be a prognostic, rather than assigned, model quantity that depends on leaf nitrogen and environmental conditions.

### 3.4 Model simulations

We assess the soil moisture relationships to carbon and water fluxes using single-point CLM5-BGC simulations with two different hydraulic strategies: (1) the Medlyn stomatal conductance model combined with the PHS model (the default option in CLM5) (CLM5-PHS) and (2) the Ball-Berry model coupled with the SMS model (CLM5-SMS). Both runs used the same meteorological forcing and vegetation and soil parameters. The two runs differed only in the stomatal conductance and the soil water stress models. For the point simulations at each Fluxnet site, we conducted a 400 model-year CLM5-BGC spinup run cycling over each site's meteorological forcings. The 400 model-years were partitioned as 100 years in an accelerated spinup mode and 300 years in normal mode. We then ran the two different parameterizations simulations initialized with the final model state of the spinup run.

### 4. Model Evaluation

SMAP L3SMPE soil moisture during the summer (June-July-August; JJA) shows relatively dry soils (10-20% SWC) in the temperate to boreal transition region in North America (36-58°N,79-108°W), with higher moisture retrieval regions removed due to vegetation water content (VWC) data flags (Figure 1). The VWC flags typically mask out SMAP retrievals in forested regions, where water content in the canopy interferes with the retrieval of soil moisture at the surface.

Using satellite-derived SMAP and in situ observations from Fluxnet (Section 2.2) and US CRN stations (Section 2.3), we compare the observed and simulated monthly climatologies of individual sites to understand the model simulation of soil moisture (Figure 2). Of the

11

eight Fluxnet sites evaluated, only two sites (Turkey Point and Oak Openings) have unflagged SMAP data available due to vegetation water content. For comparison purposes, we include the retrieved SMAP data for reference at the other six sites, though these retrievals do not accurately represent surface soil moisture. We note that due to forcing data limitations, we cannot conduct CLM simulations at the same time period as the SMAP observations. However, the SMAP climatology still provides a useful point of comparison for understanding how different observational and modeling products reflect seasonal soil moisture dynamics.

At Oak Openings (Figure 2b), the in situ observations show very little seasonal range and hold nearly constant at about 20% SWC. Similarly, SMAP simulates a minimal seasonal cycle with a slight increase in the spring and a 3-5% SWC wet bias as compared to the in situ observations. Overall, both CLM point based simulations produce a similar SWC content with a slight wet bias (<5%) in the winter and a slight dry bias in the late summer.

At the Turkey Point site (Figure 2g), the in situ observations exhibit very little seasonal variability (ranging between 13 to 18% SWC) whereas SMAP shows a more dynamic seasonal range (up to 42% SWC in February), with similar values during the summer dry down and a slight dry bias during the summer (3%). Both CLM simulations show a slight seasonal cycle with winter SWC reaching up to 30% and summer values slightly wetter (5%) than the in situ observations.

For the other six Fluxnet sites, SMAP data is shown in Figure 2 but we note that these retrievals are likely biased high because of the high vegetation water content at these sites. At UMBS site (Figure 2a) and Morgan Monroe (Figure 2f), modeled soil moisture is biased high by 5-12% throughout the season but the model captures the slight summer drying at both sites. At Sylvania (Figure 2c) and Willow Creek (Figure 2e), the model overestimates the in situ seasonal cycle amplitude, with a wet bias of about 5-8% in the winter and a dry bias of about 5% in the summer at Sylvania and up to 10% at Willow Creek. At the Old Aspen DBF site (Figure 2d) and Old Black Spruce Site (Figure 2i), the model simulates a more extreme winter wet bias of about 25% at Old Aspen and up to 35%

12

at Old Black Spruce, though we note that frozen ground may influence the in situ observations at the site, with improved agreement during the summer months at the Old Aspen site and a slight dry bias (about 5%) at the Old Black Spruce site.

At the two USCRN sites with unflagged SMAP data (Shabbona and Goodridge; Figure 2i and 2j), CLM captures the seasonal in-situ observations, while SMAP consistently underestimates observed soil moisture by on average 13%. Both of these sites represent crop land cover types and this may be a factor in the SMAP dry bias present at these sites, as a dry bias over cropland has been observed in the US Corn Belt [*Walker et al.*, 2019] and is this represents a different ecosystem than the Fluxnet sites described above.

To summarize these differences in the observations and model versions, Figure 3 compares the JJA in situ surface soil moisture data from Fluxnet sites and SMAP (noting that six of the eight sites have flagged SMAP retrievals) to the two CLM point simulations (CLM5-PHS and CLM5-SMS). Generally, CLM5-PHS simulates a slightly drier surface SWC. Overall, there is no consistent JJA bias in the model at the DBF and ENF sites, with some sites exhibiting a wet bias (UMBS, Old Aspen, Turkey Point) and others a dry bias (Sylvania, Willow Creek, Old Black Spruce). Two of the sites (Oak Openings and Morgan Monroe) have CLM points simulations that capture the median summer surface soil moisture within a few percent.

## 5.0 Simulation of water and carbon annual cycles
## 5.1 Latent Heat

Figure 4 evaluates the simulated latent heat flux from the two CLM model point-based versions (CLM5-SMS and CLM5-PHS) with Fluxnet observed fluxes for the six deciduous forest sites and the two evergreen needleleaf forest sites for the peak growing season (JJA). At the six deciduous sites, the model simulations show three different behaviors. At two of the DBF sites (Oak Openings and Old Aspen), both CLM model simulations underestimate the mean JJA latent heat flux by 15-50 W m$^{-2}$ (or 15-50%), with a greater underestimation across all sites by CLM5-SMS. At two DBF sites (UMBS and Morgan Monroe), simulated latent heat fluxes are close to the observed fluxes, with CLM5-PHS

13

showing greater agreement at UMBS and CLM5-SMS showing greater agreement at Morgan Monroe. At the remaining two DBF sites (Sylvania and Willow Creek), both model versions overestimate the observed latent heat fluxes by 15-30 W m$^{-2}$ with larger biases for CLM5-PHS. At all DBF sites, CLM5-PHS simulates slightly higher latent heat fluxes than CLM5-SMS, suggesting that the new plant hydraulic stress model enhances latent heat fluxes in this ecosystem type. For the ENF sites, the Old Black Spruce site shows minimal bias (e.g., less than 5 W m$^{-2}$) and the Turkey Point site simulations overestimate latent heat flux by 20-25 W m$^{-2}$ for the CLM5-PHS and CLM5-SMS, respectively. For the ENF sites, there is less variability between the two CLM versions, which may be due to reduced hydraulic sensitivity in these ecosystems.

Over the seasonal cycle (Figure 5), the JJA biases are apparent throughout the growing season. Generally, CLM5-PHS simulates more latent heat throughout the growing season at the DBF sites, with little difference between the two model versions at the ENF sites. With respect to the annual onset and termination of the latent heat annual cycle, the two sites that underestimate the peak growing season latent heat (Oak Openings and Old Aspen) capture the timing of the seasonal cycle fairly well, while the sites with positive JJA biases (Willow Creek, Sylvania) simulate higher fluxes in the winter than observed and often simulate an earlier onset to higher latent heat fluxes observed as the vegetation becomes active. For the two ENF sites, there is little difference between the CLM treatment of stomatal conductance and soil moisture stress. The Turkey Point site shows a slight overestimate in latent heat as noted above, while the Old Black Spruce site simulations show an unusual early spring peak in both model simulations that is not observed. Because the CLM is using point-based observations as the meteorological driver, we cannot attribute this to meteorological conditions such as temperature or solar radiation variations, and further work is needed to understand the driver of the early onset of latent heat fluxes.

The simulated biases in latent heat can be related to surface soil moisture to understand the possibility for soil moisture controls on fluxes (Figure 6). At some sites, the site observations indicate a seasonal cycle in the soil moisture-latent heat relationship, with

14

higher soil moisture in early summer (June) when latent heat fluxes are lower, transitioning to higher fluxes and lower soil moisture content in July, followed by late summer drying and lower latent heat fluxes in August. Two exceptions to this observed seasonal pattern are at the Oak Openings site, which shows a very limited range of in situ soil moisture observations (16-20% SWC), and at Turkey Point that exhibits a similar low soil moisture content range (8-11% SWC). Both CLM model simulations roughly capture the seasonal relationship, with a stronger seasonal cycle at some sites (e.g., Old Aspen, Morgan Monroe) than others (UMBS, Willow Creek). Consistent with the above analysis, the DBF sites simulate higher latent heat in CLM5-PHS, although the simulations for ENF sites do not show large model differences. For the DBF sites, this increased latent heat flux by CLM5-PHS drives the surface soil moisture to slightly drier values (e.g., shifting the seasonal curve to the left with lower SWC), suggesting a stronger soil moisture-latent heat feedback in the model for this ecosystem type.

We note that the vegetation types selected here will likely access deeper layers of soil moisture than just the surface layer based on their root structures. Although root zone soil moisture observations are not available either in situ or from SMAP Level 3 products, we did evaluate the same relationships in Figure 6 with the CLM and SMAP L4 modeled root zone soil moisture (Figure S1). The relationships that presented with the root zone soil moisture exhibited the same seasonal cycle and site-to-site variability as the surface soil moisture relationships. This may be because the root zone soil moisture does not influence the fluxes as modeled by the CLM and SMAP L4 despite the potential for greater water access, or because the relationship between root zone soil moisture and surface fluxes is highly correlated with the behavior of the surface soil moisture.

Taken together with the surface soil moisture evaluation in Section 4.0, we can draw some inferences about the latent heat flux dependence on soil moisture. Two of the sites with dry soil moisture biases (Sylvania and Willow Creek) exhibit positive latent heat flux anomalies, suggesting excessive simulated latent heat fluxes could draw down modeled soil moisture , illustrating coupling between the model canopy processes and soil moisture. Conversely, two locations with wet soil moisture biases (UMBS:CLM5-SMS and Old Aspen)

15

also show negative latent heat flux biases, suggesting that these sites are retaining more moisture in the soil instead of transpiring it to the atmosphere. Interestingly, the CLM5-PHS simulation at UMBS shows an improvement in the latent heat flux bias, while also reducing the wet soil moisture bias, suggesting that the PHS coupling is working effectively at this site. Some locations with a good representation of soil moisture (e.g., Morgan Monroe, Old Black Spruce) also show minimal latent heat flux biases, yet we note that this does not hold for all sites (e.g., Turkey Point site has only a small wet soil moisture bias yet overestimates latent heat fluxes, while Oak Openings has a slight dry soil moisture bias yet underestimates latent heat fluxes). These findings suggest that for latent heat flux, the representation of soil moisture can be important for reducing biases in surface energy fluxes.

## 5.2 Gross Primary Production (GPP)

Both CLM5-SMS and CLM5-PHS model formulations underestimate GPP compared to Fluxnet observations at five of the eight sites (Figure 7), with the exception of the Turkey Point, Sylvania and Willow Creek sites. Among DBF sites, mean JJA GPP observational estimates span the range from 5 gC m$^{-2}$ d$^{-1}$ to 13 gC m$^{-2}$ d$^{-1}$, whereas the simulated range is smaller by a factor of two. The lack of model dynamic range means that for sites with the lowest observed GPP (Sylvania, Willow Creek, and Turkey Point), the CLM simulations exhibit a low but positive bias. At the other DBF sites, the JJA average GPP bias is substantial, with GPP underestimated by up to 50%. For DBF sites, there is not a consistent GPP difference between the SMS and PHS formulations, despite that CLM5-PHS consistently simulated higher latent heat fluxes, indicating differences between the two models in water use efficiency.

The JJA bias in GPP is evident when examining the annual cycle of observed and simulated GPP (Figure 8). At most sites, the GPP observations peak around day 180, but both CLM5-PHS and CLM5-SMS peak earlier (around day 120-150), and generally decrease linearly until almost day 300, when GPP abruptly transitions to zero. Given the different seasonal shapes of the observed and simulated GPP, the largest mismatches occur during peak

16

summer for the DBF sites. At the two ENF sites, the CLM simulated growing season onset is too early and too fast in both CLM5-SMS and CLM5-PHS, with the greatest model bias in spring. We also examine the SMAP L4 GPP climatology, and find that the L4 product produces a similar seasonal cycle to the observations at the DBF sites (mid-season maxima of 8-15 gC m$^{-2}$ d$^{-1}$) with an earlier spring onset and overall a longer growing season. At some sites (UMBS, Morgan Monroe and Oak Openings), the L4 seasonal cycle provides a close match to the observations, yet other DBF sites show both positive (US-Syv and US-WCr) and negative (CA-Oas) model biases. Similarly for the ENF sites, the SMAP L4 simulations at the Turkey Point site overestimate the GPP seasonal peak by a factor of three, while the SMAP L4 provides a good match to the Fluxnet observations at the Old Black Spruce site.

The observations reveal that the seasonality in GPP and latent heat are decoupled in the CLM. Specifically, as soil moisture dries from June to August at the DBF sites (e.g., high in the spring and declining through summer), the observed GPP and LH start low in spring, peak at the transition from spring to summer, and then decline through summer and fall similar to simulated soil moisture. However, in both CLM simulations, the GPP is simulated to be higher in the spring, creating more of a linear relationship (Figure 9). Because the LH shows a similar seasonal cycle as the observations (relatively low in June, increasing in July and then decreasing in August) and the GPP does not, this suggests that the GPP and LH are uncoupled during spring in the model. In contrast, the SMAP L4 data reproduces the observed behavior when accounting for the noted soil moisture and GPP biases, and simulates the spring low GPP in a more realistic manner. Similar to the latent heat results, these relationships do not change substantially when regressing the GPP against the root zone soil moisture (Figure S2). These results suggest, unsurprisingly, that factors other than soil moisture, such as radiation or phenology, likely control GPP during spring. In contrast, the simulated GPP during summer and fall seems to be linearly related to soil moisture. The GPP-soil moisture relationship is weakest at the University of Michigan Biological Station (Figure 9a), which is among the driest sites.

**6.0 Discussion**

17

The evaluation of land surface models with in situ land surface data is inherently limited due to sparse spatial observations of surface processes and the high degree of land surface heterogeneity. The use of satellite-derived products such as SMAP may be useful in filling this spatial gap, as such products provide an unprecedented spatial scale to observe a quantity such as soil moisture. However, there are limitations to the satellite data, as the water content in the canopies can interfere with retrievals of water at the surface in densely vegetated regions such as forest or shrub. This leads to broad regions of SMAP data being removed due to interference from high VWC. To fill these gaps, we utilize other data sets (Fluxnet and US-CRN observations, SMAP L4 modeled soil moisture and fluxes) to draw broader conclusions about the challenges of understanding the role of soil moisture on the fluxes of water and carbon from vegetation.

One confounding aspect of our study is that no single variable accounts for the majority of the site-to-site variability, especially for GPP. We synthesized our results in Figure 10, which notes the relative temperature and radiation differences between the sites as well as the model biases for latent heat and GPP as compared to Fluxnet observations. From Figure 1, the latitudinal gradient of sites is supported by the annual average temperatures and shortwave radiation (Table 1 and Figure 10). The lowest latitude sites (Morgan Monroe, Oak Openings, and Turkey Point; Figure 10a-c) have the warmest temperatures (>20°C) and highest radiation (>430 W m$^{-2}$), while a second cluster includes three sites (Willow Creek, Sylvania and UMBS; Figure 10d-f) with slightly cooler temperatures (17-19°C) and moderate radiation (around 400-410 W m$^{-2}$). The highest latitude group of sites (CA-Oas and CA-Obs; Figure 10g-h) have the lowest temperatures (~15°C) and radiation (340-350 W m$^{-2}$).

Within a plant functional type (e.g., DBF), these groupings by climate zone do not have a consistent impact on the latent heat biases (Figure 4), as warmer sites with more radiation (Morgan Monroe, Oak Openings) do not have substantially different latent heat fluxes than the next climate zone (including Willow Creek, Sylvania and UMBS). Some of the sites in

18

the warmer latitudes have positive latent heat flux biases (e.g., Sylvania, Willow Creek, and Turkey Point), while others simulate negative latent heat fluxes biases (e.g., Oak Openings, and UMBS). Additionally dry soil moisture biases at some sites (Morgan Monroe, Oak Openings, Sylvania and Willow Creek) lead to positive latent heat flux biases at some sites (Sylvania and Willow Creek), negative latent heat flux biases at others (Oak Openings), and a split bias at Morgan Monroe with the PHS model version driving higher latent heat fluxes. Two of the sites have slightly wet biases (Turkey Point and UMBS), with positive latent heat flux biases at one site (Turkey Point) and a split response at the other site (UMBS, again with the PHS model simulating more latent heat flux). As noted in section 5.1, the soil moisture biases can often be connected with the latent heat flux biases, and the CLM5-PHS configuration appears to improve this coupling at some sites.

Lower modeled fluxes are evident at the Old Aspen site, which may be a function of the lower solar radiation and cooler temperatures, but this is not supported by the observations that show latent heat fluxes similar to the other climate zones (approximately 60-90 W m$^{-2}$; Figure 4). The influence of temperature and radiation on GPP is not directly related, as higher latitude sites such as Old Aspen have similar GPP to that of sites at lower latitudes (e.g., UMBS and Morgan Monroe). However, we again highlight the minimal variability in the CLM simulated GPP between the DBF sites. The Old Aspen and Old Black Spruce sites show positive and negative soil moisture biases, respectively, yet both sites show negative biases for both latent heat flux and GPP. In addition, the flux biases are more negative for the Old Aspen site, despite it having a wet soil moisture bias. Overall, this suggests that the soil moisture coupling in the CLM5 point simulations is extremely weak at these high latitude sites.

In addition to climate variables, other site-dependent parameters used in the CLM model may influence the site-to-site variability. We note that most of the plant physiological parameters in CLM (e.g., $g_1$ in the stomatal conductance parameterization (Equation 1), $\beta$ in the soil moisture function (Equation 2)) do not vary between the temperate and boreal forests, and this could be one area for future investigation to determine if site specificity in

19

these parameters could improve the representation of surface fluxes. Additionally, the model simulations are extremely sensitive to the leaf area index (LAI). While we use the LAI simulation developed in the CLM BGC mode, we note that other gridded simulations that use a different formulation for LAI provide very different results, with fluxes that tend to be somewhat higher than that from the point simulations (results not shown). As a result, we suggest that careful attention be paid to the simulation of LAI by land surface models that are estimating water and carbon fluxes.

New parameterizations within the CLM have expanded the definitions of how plants utilize soil water, and the PHS parameterization [*Kennedy et al.*, 2019] utilized with the Medlyn stomatal conductance model provides a theoretically consistent mechanism for simulating water stress in land surface models. Our results show that the PHS model generally tends to change soil moisture and fluxes across all sites, simulating higher latent heat fluxes and lower soil moisture (Fig. 3-4). This change can alleviate the latent heat flux bias in some locations (e.g., Oak Openings, Turkey Point, UMBS and Old Aspen), yet at other sites it can exacerbate the bias (Morgan Monroe, Sylvania and Willow Creek) (Figure 10). At all sites, this change in hydraulic strategy had little impact on the simulated GPP magnitude or the model bias.

An interesting result from our CLM5 simulations is that the observed and simulated seasonal cycles of GPP and latent heat fluxes are different, especially at DBF sites. This suggests that stomatal conductance is not the only factor that regulates rates of photosynthesis and latent heat fluxes for any given soil moisture level. The shape of the latent heat flux is more consistent with energy limitation early in the year, because at most sites the peak is between day 180 and 210. The annual cycle is more symmetric for latent heat than it is for GPP (Fig. 5 vs Fig. 8), suggesting that radiation may also be an important control on late summer and fall latent heat as well. In contrast, the climatology of GPP fluxes appears to be much more closely coupled to soil moisture. Phenology, coupled with radiation limitation, likely regulates the rate of GPP increase in spring and early summer, but after GPP peaks around day 180, the DBF sites show a nearly linear decrease in GPP. At least during July and August, this results in GPP being linked with the seasonal decline in

20

soil moisture (Fig. 9). Taken with the close linkages between summer soil moisture drying and the trajectory in GPP in CLM, this suggests that additional attention to accounting for canopy properties such as LAI may be more important than accounting for soil moisture in improving model simulations of carbon and water fluxes.

One potential path forward to increase the utility of the SMAP data to the Earth System modeling community could be to re-examine the derivation of the VWC. For example, the current development of the VWC is based on accounting for water in the canopy (canopy water content) and the stems of leaves (stem water content). While the canopy water content is based on satellite-derived Normalized Difference Vegetation Index (NDVI), the stem water content is based on the wood content of vegetation, which dominantly driven by values assigned by plant functional type [*Chan et al.*, 2013]. This leads to a relatively high value of stem water content, and subsequently VWC for all forested types has minimal seasonal variation. Potential paths to work around this challenge could include re-examining this relationship in the winter months when water content tends to be stored below ground, or the use of microwave remote sensing products to derive vegetation water content [*Konings et al.*, 2019]. Without a way to account for the seasonality of water stored within the forest canopy, it remains challenging to utilize SMAP in densely forested regions.

Taken together, the lack of clear mechanistic control of environmental variables on surface energy and carbon fluxes presents a challenging point for the community. While physical parameterizations such as those in the CLM represent our best understanding of physical processes in a forest canopy, our work highlights the spatial variability between Fluxnet sites within the same PFT and climatic zones, as well as the shortcomings of the model to reproduce the observed spatial and temporal variability. It is possible that these questions may be able to be explored at a broader scale using new satellite products such as GEDI [*Dubayah*, 2020] or ECO-STRESS [*Fisher*, 2020] to elucidate some of the underlying assumptions in the physical parameterizations.

**7.0 Conclusions**

21

Soil moisture is an important environmental driver for land surface processes, yet remains poorly constrained in land surface models [*Koster et al.*, 2009]. Validated land surface data, including soil moisture and surface heat fluxes, are difficult to obtain on broad spatial scales yet are crucial for understanding the role of the land surface in the Earth system. In this paper, we explore the use of new satellite-derived soil moisture data to compare with sparse in situ observations of surface processes and a land surface model that utilizes different parameterizations of water access in the canopy.

Our analysis reveals that CLM point-based simulations at deciduous flux tower sites are characterized by both dry and wet biases, suggesting that site-to-site variability may play a more important role than ecosystem or canopy type. Biases in soil moisture can be connected to biases at latent heat fluxes at most sites, indicating that improvement of soil moisture will have an important impact on the simulation of surface energy fluxes. However, some sites do not show a clear relationship between latent heat flux and soil moisture, suggesting that these processes may be uncoupled in some ecosystems. For carbon fluxes, the SMAPL4 data appears to capture the seasonal cycle better than the CLM simulations, but the site-to-site differences cannot be fully explained.

Because root zone observations of soil moisture are difficult to obtain, we rely on the models to understand relationships between the deeper soil moisture available to roots and fluxes at the surface. Overall, these modeled relationships do not vary greatly between the surface versus root zone regressions, although this result is difficult to verify given the limited availability of in situ soil moisture data the Fluxnet sites. Accounting for climate (temperature, solar radiation) and vegetation (plant functional type), we could identify no unique variable that could comprehensively disentangle these site-to-site differences. Although our expectation was that latent heat fluxes and GPP would be tightly coupled via stomatal regulation, modeled GPP is uncoupled from latent heat seasonal changes in CLM. Results from the SMAP L4 product show less site-to-site variability than the CLM5 data, with positive or negative biases at different sites. These findings suggest that observed site-to-site variability of water and carbon fluxes cannot be explained by current model parameterizations. Further work that evaluates these point simulations versus

22

gridded CLM simulations would be useful, particularly ones that consider the use of prognostic versus prescribed leaf area index.

This highlights the need for further focus on understanding the coupling between soil moisture and water and carbon fluxes, as the models do not accurately represent the observed relationships between carbon and water.  As noted by [*Koster et al.*, 2009], most land surface models capture the temporal variability of soil moisture, but the magnitude of soil water can vary greatly between individual models.   Because many of these land surface models are derived from the same first principles and soil moisture is essentially a "free" variable in Earth System Models, it is perhaps not surprising that inter-model comparisons may converge on an accurate seasonal cycle yet still diverge in magnitude. The work presented here confronts how well models capture not just the soil moisture magnitude, but also how the models capture the observed relationships that feedback to surface fluxes.  We find that one of the main models of the land surface modeling community struggles to capture these observed relationships at forested sites.  This suggests that future model development would be greatly enhanced by utilizing soil moisture observations from multiple sites and spatially from remote sensing, with the goal of capturing these essential coupled processes.  Overall, the results we present here prompts future analysis of factors that regulate land-atmosphere carbon and water exchange in tandem with soil moisture controls, and new satellite data that will provide evapotranspiration and canopy structure at the global scale may be helpful in elucidating these important mechanisms.

Management Project, and Fluxdata project of FLUXNET, with the support of CDIAC and ICOS Ecosystem Thematic Center, and the OzFlux, ChinaFlux and AsiaFlux offices. US CRN data are available at https://www.ncdc.noaa.gov/crn/qcdatasets.html in the Daily01 and Hourly02 subdirectories. SMAP satellite-derived surface soil moisture data and L4 data are available from the National Snow and Ice Data Center following registration. The CRUNCEP Version 7 atmospheric forcing data used to force CLM5 are provided by NCAR's Computational and Information Systems Laboratory at http://rda.ucar.edu/datasets/ds314.3. The database of the CLM model simulations described in this study is available at the University of Michigan Deep Blue data archive (https://deepblue.lib.umich.edu/data/concern/data_sets/0p096696q?locale=en).

24

**Table 1.** Location, PFT, soil type and number of years of atmospheric forcing for each Fluxnet site used for model evaluation. Biome types include deciduous broadleaf forest (DBF) and evergreen needleleaf forest (ENF).

| Site ID | Name | Lon. (° E) | Lat. (° N) | Elev (m) | IGBP Biome type | Model Prescribed vegetation type | Soil texture (%sand, %clay and %silt) and organic content (kg OM m$^{-3}$) | Site-years available | Annual Ave T(K) | Annual Ave. Radiation (W m$^{-2}$) |
|---|---|---|---|---|---|---|---|---|---|---|
| CA-Oas[1] | Western Boreal Mature Aspen | -106.19 | 53.63 | 530 | DBF | DBF Boreal | 48.6, 10.1, 41.3, 130 | 1996-2010 (15) | 15.4 | 351.0 |
| CA-Obs[2] | Western Boreal Mature Black Spruce | -105.11 | 53.99 | 629 | ENF | ENF Boreal | 72.8, 5.8, 21.4, 130 | 1997-2010 (14) | 15.1 | 343.5 |
| CA-TP1[3] | Turkey Point 2002 Plantation White Pine | -80.55 | 42.66 | 265 | ENF | ENF temperate | 98.0, 0.0, 2.0, 18.4 | 2002-2014 (13) | 20.4 | 451.9 |
| US-MMS[4] | Morgan Monroe State Forest | -86.41 | 39.32 | 275 | DBF | DBF temperate | 34.0, 63.0, 3.0, 83.5 | 1999-2014 (16) | 23.4 | 444.3 |
| US-Oho[5] | Oak Openings | -83.84 | 41.55 | 320 | DBF | DBF temperate | 95.0, 5.0, 0.0, 37.4 | 2004-2013 (10) | 21.6 | 431.1 |
| US-Syv[6] | Sylvania Wilderness Area | -89.34 | 46.24 | 540 | MF | 60% DBF boreal and 40% ENF boreal | 57.0, 6.0, 37.0, 130 | 2001-2014 (14) | 17.0 | 411.2 |
| US-UMB[7] | Univ. of Michigan Biological Station | -84.71 | 45.56 | 234 | DBF | DBF temperate | 92.6, 0.6, 6.8, 130 | 2000-2014 (15) | 18.8 | 401.2 |
| US-WCr[8] | Willow Creek | -90.07 | 45.80 | 520 | DBF | DBF temperate | 54.0, 13.0, 33.0, 130 | 1999-2014 (16) | 18.3 | 398.5 |

[1] Griffis et al., 2004 [2] Bergeron et al., 2007 [3] Arain & Restrepo-Coupe, 2005 [4] Schmid et al. 2000 [5] DeForest et al 2006 [6] Desai et al. 2005 [7]Curtis et al., 2002 [8] Cook et al., 2004

25

**Figure Captions**

**Figure 1.** Spatial distribution of 2015 average summer (JJA) surface soil moisture (first 5 cm; %SWC) based on the SMAP L3SMPE product . Stippling regions indicate vegetation water content above 5 kg m$^{-2}$ for the temperate-to-boreal transition region of North America (36-58°N,79-108°W).

**Figure 2.** Monthly climatologies of soil moisture (%SWC) for in-situ observations (Fluxnet and USCRN sites; 2004-2010), CLM simulations (2004-2010), and SMAP estimates (April 2015-November 2018). Error bars represent the range of one standard deviation.

**Figure 3.** Summer (JJA) box and whisker plot (line, median; box, interquartile range) of surface soil moisture (approximately the first 5 cm; %SWC) from Fluxnet observations (grey), CLM5-SMS (red) and CLM5-PHS (blue) simulations (2004-2010), and SMAP estimates (April 2015-November 2018). Whiskers extend to 1.5 times the interquartile range, with dots outside of the whiskers showing outliers. The vertical dashed line separates DBF sites (left) from ENF sites (right). For each biome type, sites are ordered by median observed soil moisture from left (more dry) to right (more wet).

**Figure 4.** Summer (JJA) box and whisker plot (line, median; box, interquartile range) of latent heat flux (W m$^{-2}$) from Fluxnet observations (grey), CLM5-SMS (red) and CLM5-PHS (blue) simulations (2004-2010). Whiskers extend to 1.5 times the interquartile range, with dots outside of the whiskers showing outliers. The vertical dashed line separates DBF sites (left) from ENF sites (right). For each biome type, sites are ordered by median observed soil moisture from left (more dry) to right (more wet).

**Figure 5.** Mean annual (2004-2010) seasonal cycle (lines) and 95% confidence intervals (gray envelopes) for observed Fluxnet (black), and simulated CLM5-SMS (red) and CLM5-PHS (blue) latent heat flux (W m$^{-2}$). Sites are ordered from dry to wet, and arranged as DBF (top and center rows) and ENF (bottom row).

**Figure 6.** Observed (grey; Fluxnet) and simulated CLM5-SMS and CLM5-PHS (red and blue) relationship between latent heat (W m$^{-2}$) and soil moisture (%SWC). Data are based on daily climatologies for June (squares), July (triangles) and August (circles) from 2004-2010.

**Figure 7.** Same as Figure 4, but for GPP (g C m$^{-2}$ d$^{-1}$).

**Figure 8.** Same as Figure 5, but for GPP (g C m$^{-2}$ d$^{-1}$). SMAP L4 climatological GPP (orange) is included for the time period April 2015-November 2018.

**Figure 9.** Same as Figure 6, but for GPP (g C m$^{-2}$ d$^{-1}$). SMAP L4 climatological GPP (orange) is included for the time period April 2015-November 2018.

**Figure 10.** Summary of site climatological conditions and model biases. Site-to-site differences in annual average temperature ($\Delta$T;K) and annual average incoming solar

26

radiation ($\Delta R$; W m$^{-2}$) represent the variability in site conditions from the observed mean of 8 Fluxnet sites, indicating sites that are relatively warmer or cooler or receive more or less radiation. Site biases for JJA mean latent heat (W m$^{-2}$) and GPP (g C m$^{-2}$ d$^{-1}$) are presented as the difference between CLM and Fluxnet observations at individual sites.

27

## References

Baldocchi, D. D., and K. B. Wilson (2001), Modeling CO2 and water vapor exchange of a temperate broadleaved forest across hourly to decadal time scales, Ecological Modelling, 142(1-2), 155-184, doi: 10.1016/s0304-3800(01)00287-3.

Ball, J. T., I. E. Woodrow, and J. A. Berry (1987), A Model Predicting Stomatal Conductance and its Contribution to the Control of Photosynthesis under Different Environmental Conditions, in Progress in Photosynthesis Research, edited by J. Biggins, Springer, Dordrecht.

Bell, J. E., M. A. Palecki, C. B. Baker, W. G. Collins, J. H. Lawrimore, R. D. Leeper, and e. al. (2013), U.S. Climate Reference Network Soil Moisture and Temperature Observations, Journal of Hydrometeorology, 14(3), doi: 10.1175/jhm-d-12-0146.1.

Bonan, G. B., P. J. Lawrence, K. W. Oleson, S. Levis, M. Jung, M. Reichstein, D. M. Lawrence, and S. C. Swenson (2011), Improving canopy processes in the Community Land Model version 4 (CLM4) using global flux fields empirically inferred from FLUXNET data, J. Geophys. Res.-Biogeosci., 116, doi: 10.1029/2010jg001593.

Bryan, A. M., A. L. Steiner, and D. J. Posselt (2015), Regional modeling of surface-atmosphere interactions and their impact on Great Lakes hydroclimate, J. Geophys. Res.-Atmos., 120(3), 1044-1064, doi: 10.1002/2014JD022316.

Chan, S., R. Bindlish, R. Hung, T. Jackson, and J. Kimball (2013), Vegetation Water Content, Ancillary Report*Rep.*, Jet Propulsion Laboratory, Pasadena, CA.

Das, N. N., D. Entekhabi, and E. G. Nijoku (2011), An Algorithm for Merging SMAP Radiometer and Radar Data for High-Resolution Soil-Moisture Retrieval, IEEE Transactions on Geoscience and Remote Sensing, doi: 10.1109/TGRS.2010.2089526.

Dirmeyer, P. A., C. A. Schlosser, and K. L. Brubaker (2009), Precipitation, Recycling, and Land Memory: An Integrated Analysis, Journal of Hydrometeorology, 10(1), 278-288, doi: 10.1175/2008jhm1016.1.

Dubayah, R., Blair, J.B., Goetz, S., Fatoyinbo, L., Hansen, M., Healey, S., Hofton, M., Hurtt, G., Kellner, J., Luthcke, S., & Armston, J. (2020), The Global Ecosystem Dynamics Investigation: High-resolution laser ranging of the Earth's forests and topography, Science of Remote Sensing, 1, 100002, doi: 10.1016/j.srs.2020.100002.

Entekhabi, D., S. Yueh, P. E. O'Neill, K. H. Kellogg, and e. al. (2014), SMAP Handbook, edited, JPL Publication 400-1567, Pasadena CA.

Entekhabi, D., E. G. Njoku, P. E. O'Neill, K. H. Kellogg, W. T. Crow, W. N. Edelstein, and e. al. (2010), The Soil Moisture Active Passive (SMAP) Mission, Proceedings of the IEEE, doi: 10.1109/JPROC.2010.2043918.

Farquhar, G. D., S. V. Caemmerer, and J. A. Berry (1980), A BIOCHEMICAL-MODEL OF PHOTOSYNTHETIC CO2 ASSIMILATION IN LEAVES OF C-3 SPECIES, Planta, 149(1), 78-90, doi: 10.1007/bf00386231.

Fisher, J. B. e. a. (2020), ECOSTRESS: NASA's Next Generation Mission to Measure Evapotranspiration From the International Space Station, Water Resources Research, 54(8), 2019WR026058, doi: 10.1029/2019WR026058.

Franks, P. J., G. B. Bonan, J. A. Berry, D. L. Lombardozzi, N. M. Holbrook, N. Herold, and K. W. Oleson (2018), Comparing optimal and empirical stomatal conductance models for application in Earth system models, Glob. Change Biol., 24(12), doi: https://doi.org/10.1111/gcb.14445.

28

Jones, L. A., J. S. Kimball, R. H. Reichle, N. Mandani, J. Glassy, J. V. Ardizzone, and e. al. (2017), The SMAP Level 4 Carbon Product for Monitoring Ecosystem Land–Atmosphere CO2 Exchange, IEEE Transactions on Geoscience and Remote Sensing, 6517-6532, doi: 10.1109/TGRS.2017.2729343.

Jung, M., et al. (2010), Recent decline in the global land evapotranspiration trend due to limited moisture supply, Nature, 467(7318), 951-954, doi: 10.1038/nature09396.

Kennedy, D., S. Swenson, K. W. Oleson, D. M. Lawrence, R. Fisher, A. C. L. da Costa, and P. Gentine (2019), Implementing Plant Hydraulics in the Community Land Model, Version 5, Journal of Advances in Modeling Earth Systems, 11(2), 485-513, doi: 10.1029/2018ms001500.

Keppel-Aleks, G., A. S. Wolf, M. Mu, S. C. Doney, D. C. Morton, P. S. Kasibhatla, J. B. Miller, E. J. Dlugokencky, and J. T. Randerson (2014), Separating the influence of temperature, drought, and fire on interannual variability in atmospheric CO2, Global Biogeochemical Cycles, 28(11), 1295-1310, doi: 10.1002/2014gb004890.

Konings, A. G., K. Rao, and S. C. Steele-Dunne (2019), Macro to micro: microwave remote sensing of plant water content for physiology and ecology, New Phytologist, 223(3), doi: 10.1111/nph.15808.

Koster, R. D., Z. Guo, R. Yang, P. A. Dirmeyer, K. Mitchell, and M. Puma, J. (2009), On the nature of soil moisture in land surface models, J. Clim., 22(16), 4322-4335, doi: 10.1175/2009JCLI2832.1.

Lasslop, G., M. Reichstein, D. Papale, A. Richardson, A. Arneth, A. Barr, P. C. Stoy, and G. Wohlfahrt (2010), Separation of net ecosystem exchange into assimilation and respiration using a light response curve approach: Critical issues and global evaluation, Glob. Change Biol., 16(1), doi: 10.1111/j.1365-2486.2009.02041.x.

Lawrence, D., R. Fisher, C. Koven, K. Oleson, S. Swenson, M. Vertenstein, and e. al. (2019), The Community Land Model version 5: Description of new features, benchmarking, and impact of forcing uncertainty, Journal of Advances in Modeling Earth Systems, 11, doi: 10.1029/2018MS001583.

Lei, H., M. Huang, L. R. Leung, D. Yang, X. Shi, J. Mao, D. J. Hayes, C. R. Schwalm, Y. Wei, and S. Liu (2014), Sensitivity of global terrestrial gross primary production to hydrologic states simulated by the Community Land Model using two runoff parameterizations, Journal of Advances in Modeling Earth Systems, 6(3), 658-679, doi: 10.1002/2013ms000252.

Matheny, A. M., et al. (2014), Characterizing the diurnal patterns of errors in the prediction of evapotranspiration by several land-surface models: An NACP analysis, J. Geophys. Res.-Biogeosci., 119(7), 1458-1473, doi: 10.1002/2014jg002623.

Medlyn, B. E., R. A. Duursma, D. Eamus, D. S. Ellsworth, I. C. Prentice, C. V. M. Barton, K. Y. Crous, P. de Angelis, M. Freeman, and L. Wingate (2011), Reconciling the optimal and empirical approaches to modelling stomatal conductance, Glob. Change Biol., 17(6), 2134-2144, doi: 10.1111/j.1365-2486.2010.02375.x.

Mu, Q., M. Zhao, and S. W. Running (2011), Improvements to a MODIS global terrestrial evapotranspiration algorithm, Remote Sens. Environ., 115(8), 1781-1800, doi: 10.1016/j.rse.2011.02.019.

O'Neill, P. E., S. Chan, E. G. Njoku, T. Jackson, and R. Bindlish (2018), SMAP Enhanced L3 Radiometer Global Daily 9 km EASE-Grid Soil Moisture, Version 2, edited.

Oleson, K. W., D. M. Lawrence, and e. al. (2013), Technical Description of version 4.5 of the Community Land Model (CLM)*Rep.*, 434 pp, National Center for Atmospheric Research, Boulder, CO.

Reichle, R. H., G. J. M. De Lannoy, Q. Liu, J. V. Ardizzone, A. Colliander, A. Conaty, W. T. Crow, and e. al. (2017), Assessment of the SMAP Level-4 Surface and Root-Zone Soil Moisture Product Using In Situ Measurements, Journal of Hydrometeorology, 18(10), 2621-2645, doi: 10.1175/JHM-D-17-0063.1.

Rogers, A., B. E. Medlyn, J. S. Dukes, G. Bonan, S. von Caemmerer, M. Dietze, and e. al. (2017), A roadmap for improving the representation of photosynthesis in Earth system models, New Phytologist, 213(1), 22-42, doi: 10.1111/nph.14283.

Seneviratne, S. I., T. Corti, E. L. Davin, M. Hirschi, E. B. Jaeger, I. Lehner, B. Orlowsky, and A. J. Teuling (2010), Investigating soil moisture-climate interactions in a changing climate: A review, Earth-Science Reviews, 99(3-4), 125-161, doi: 10.1016/j.earscirev.2010.02.004.

Suyker, A. E., S. B. Verma, and G. G. Burba (2003), Interannual variability in net $CO_2$ exchange of a native tallgrass prairie, Glob. Change Biol., 9(2), 255-265, doi: 10.1046/j.1365-2486.2003.00567.x.

Thornton, P. E., J.-F. Lamarque, N. A. Rosenbloom, and N. M. Mahowald (2007), Influence of carbon-nitrogen cycle coupling on land model response to $CO_2$ fertilization and climate variability, Global Biogeochemical Cycles, 21(4), doi: 10.1029/2006gb002868.

Walker, V. A., B. K. Hornbuckle, M. H. Cosh, and J. H. Prueger (2019), Seasonal Evaluation of SMAP Soil Moisture in the U.S. Corn Belt, Remote Sensing, 11(21), 2488, doi: doi.org/10.3390/rs11212488.

White, M. A., P. E. Thornton, S. W. Running, and R. R. Nemani (2000), Parameterization and Sensitivity Analysis of the BIOME–BGC Terrestrial Ecosystem Model: Net Primary Production Controls, Earth Interactions, 4(3), 1-85, doi: 10.1175/1087-3562(2000)004<0003:PASAOT>2.0.CO;2.

Wozniak, M. C., G. B. Bonan, G. Keppel-Aleks, and A. L. Steiner (2020), Influence of sub-canopy microenvironment on inter-annual variability of carbon uptake in temperate deciduous forests, J. Geophys. Res.-Biogeosci., 125(8), doi: 10.1029/2020JG005658.

Xia, Y., M. T. Hobbins, Q. Mu, and M. B. Ek (2015), Evaluation of NLDAS-2 evapotranspiration against tower flux site observations, Hydrological Processes, 29(7), 1757-1771, doi: 10.1002/hyp.10299.
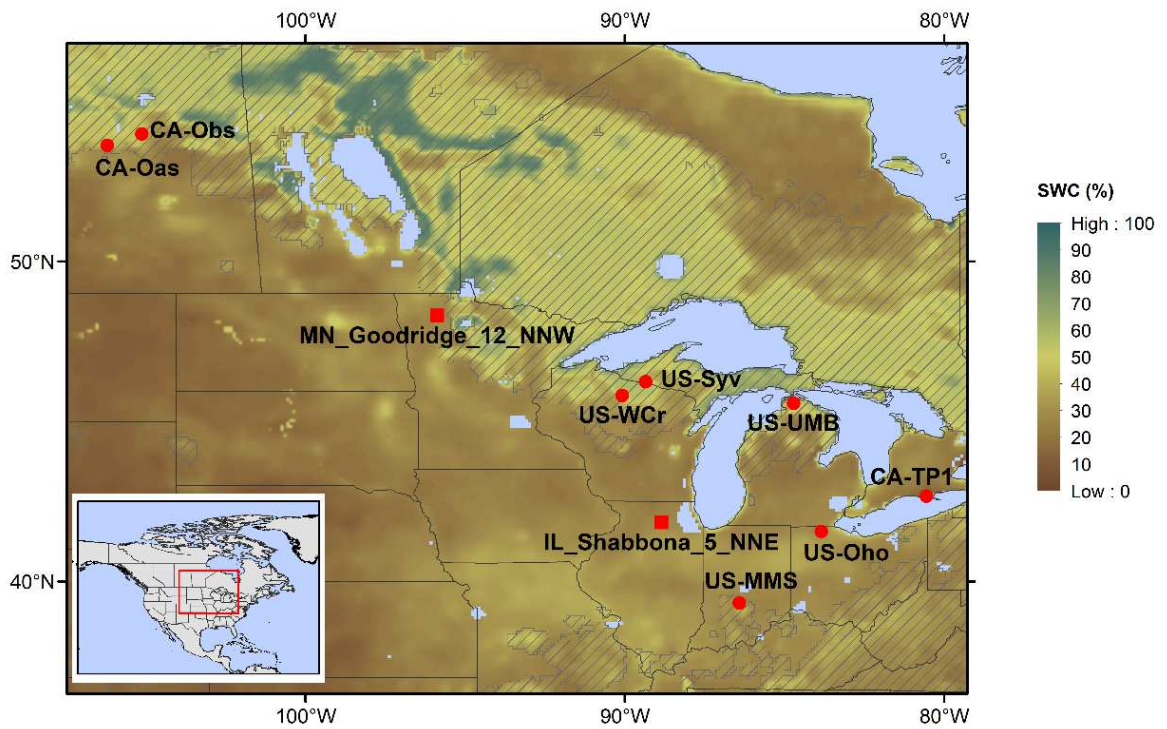
**Figure 1.** Spatial distribution of 2015 average summer (JJA) surface soil moisture (first 5 cm) based on the SMAP L3SMPE product . Stippling regions indicate vegetation water content above 5 kg m$^{-2}$ for the temperate-to-boreal transition region of North America (36-58°N,79-108°W).
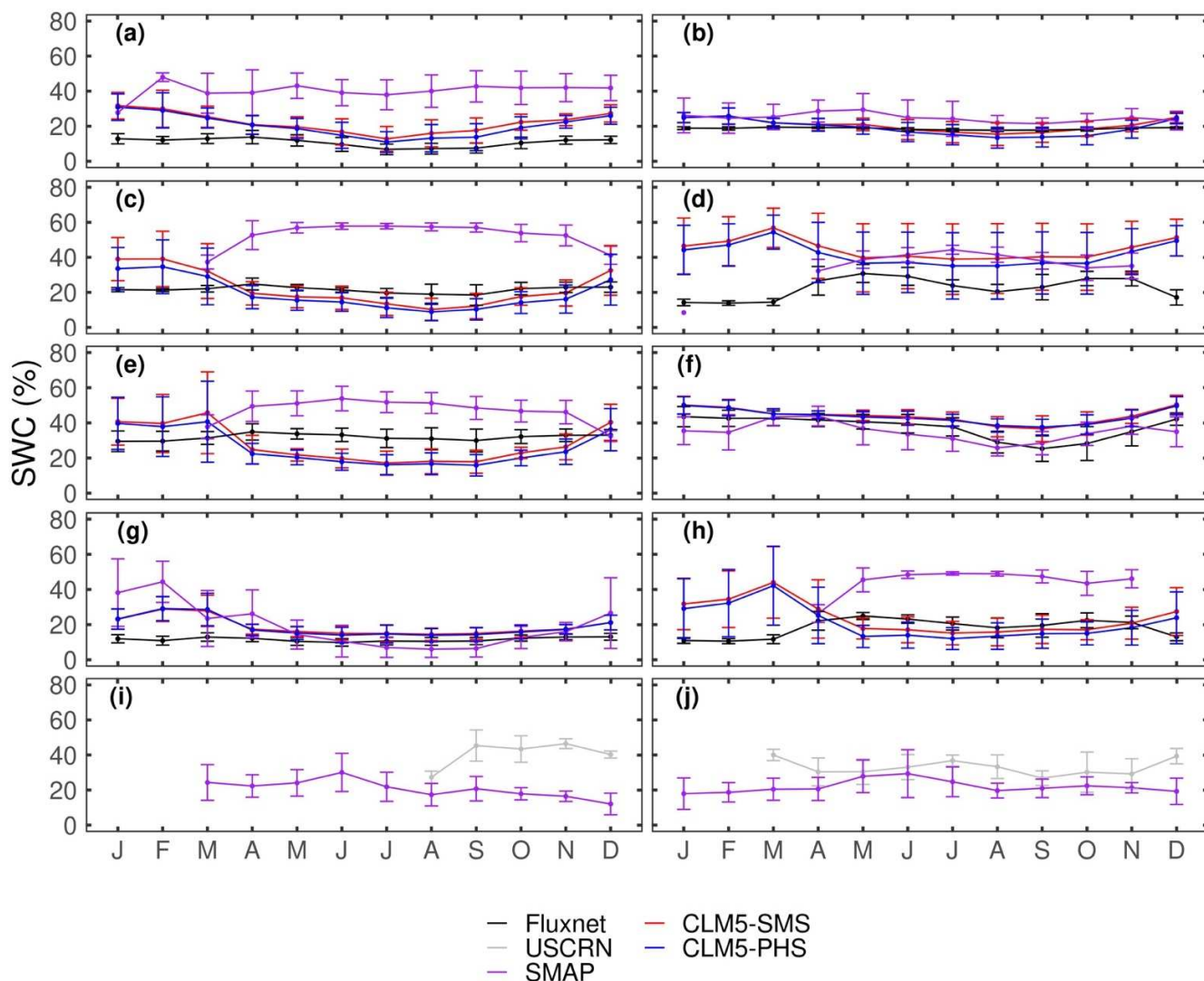
31

**Figure 2.** Monthly climatologies of soil moisture for in-situ observations (Fluxnet and USCRN sites; 2004-2010), CLM simulations (2004-2010), and SMAP estimates (April 2015-November 2018). Note that SMAP data is flagged for vegetation water content > 5 kg m$^{-2}$ at all sites except for Turkey Point and Oak Openings. Error bars represent the range of one standard deviation.
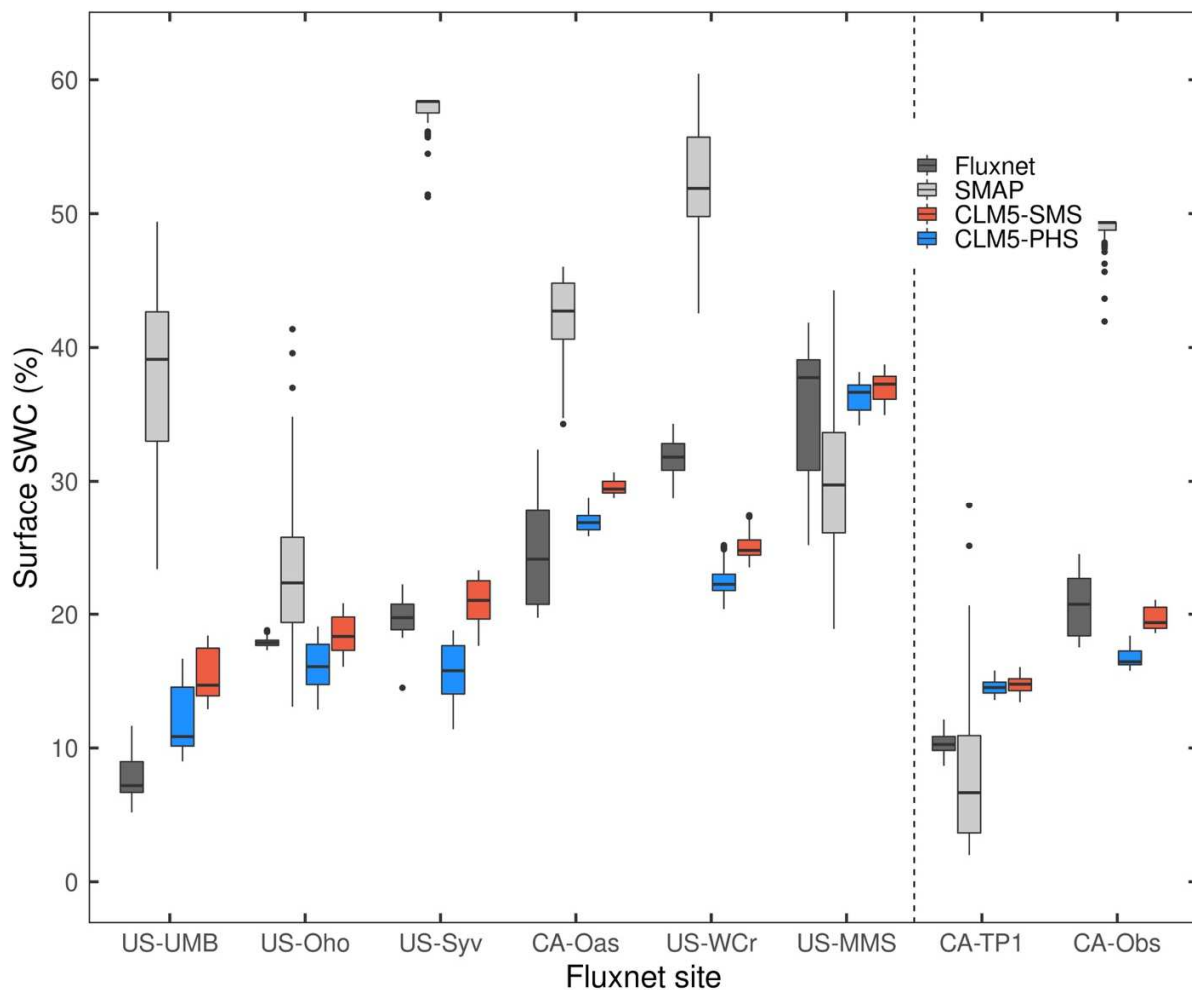
32

**Figure 3.** Summer (JJA) box and whisker plot (line, median; box, interquartile range) of surface soil moisture (approximately the first 5 cm) from Fluxnet observations (2004-2010), CLM simulations (2004-2010), and SMAP estimates (April 2015-November 2018). Whiskers extend to 1.5 times the interquartile range, with dots outside of the whiskers showing outliers. The vertical dashed line separates DBF sites (left) from ENF sites (right). For each biome type, sites are ordered by median observed soil moisture from left (more dry) to right (more wet).
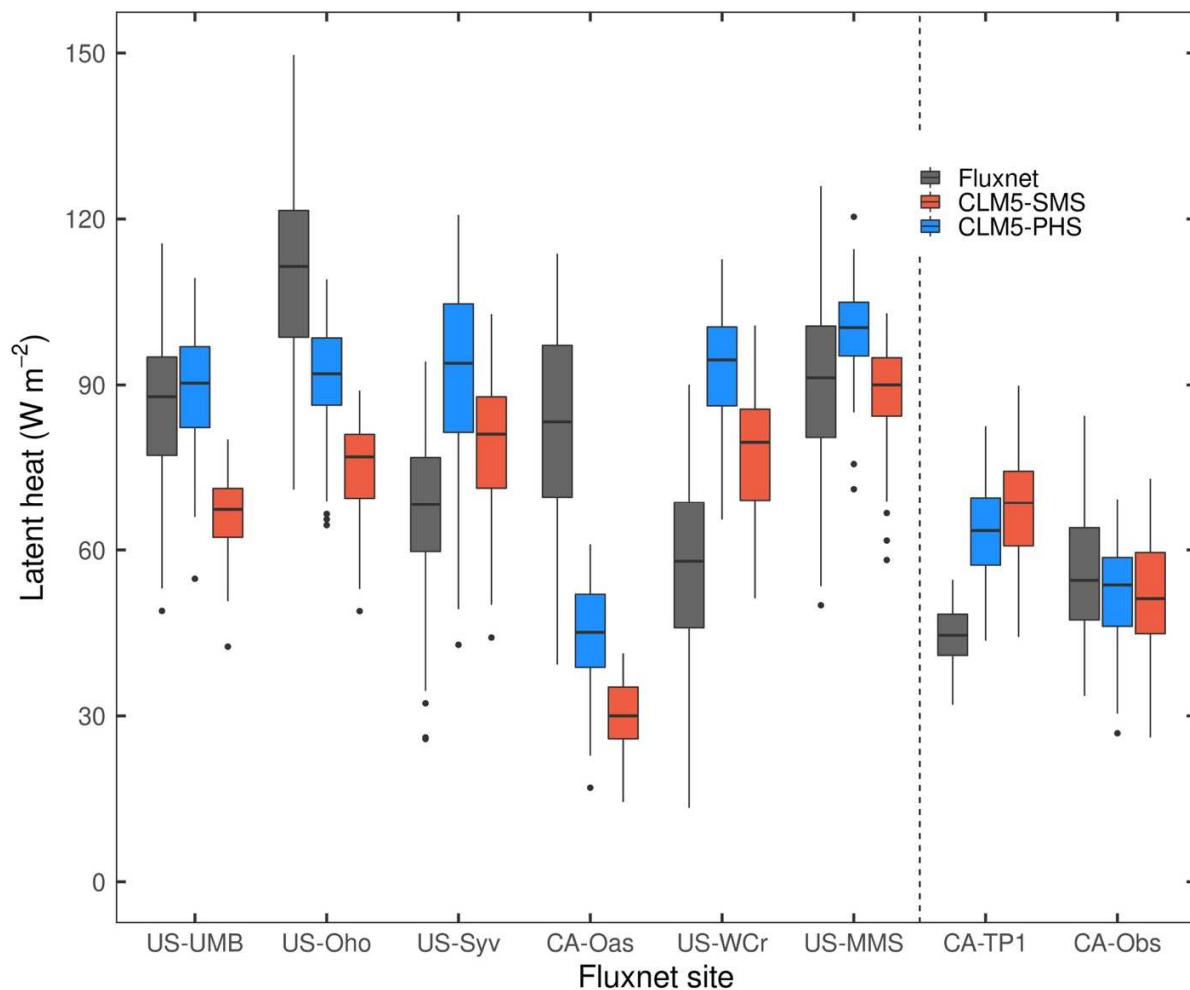
33

**Figure 4.** Summer (JJA) box and whisker plot (line, median; box, interquartile range) of latent heat flux from Fluxnet observations (2004-2010) and CLM simulations (2004-2010). Whiskers extend to 1.5 times the interquartile range, with dots outside of the whiskers showing outliers. The vertical dashed line separates DBF sites (left) from ENF sites (right). For each biome type, sites are ordered by median observed soil moisture from left (more dry) to right (more wet).
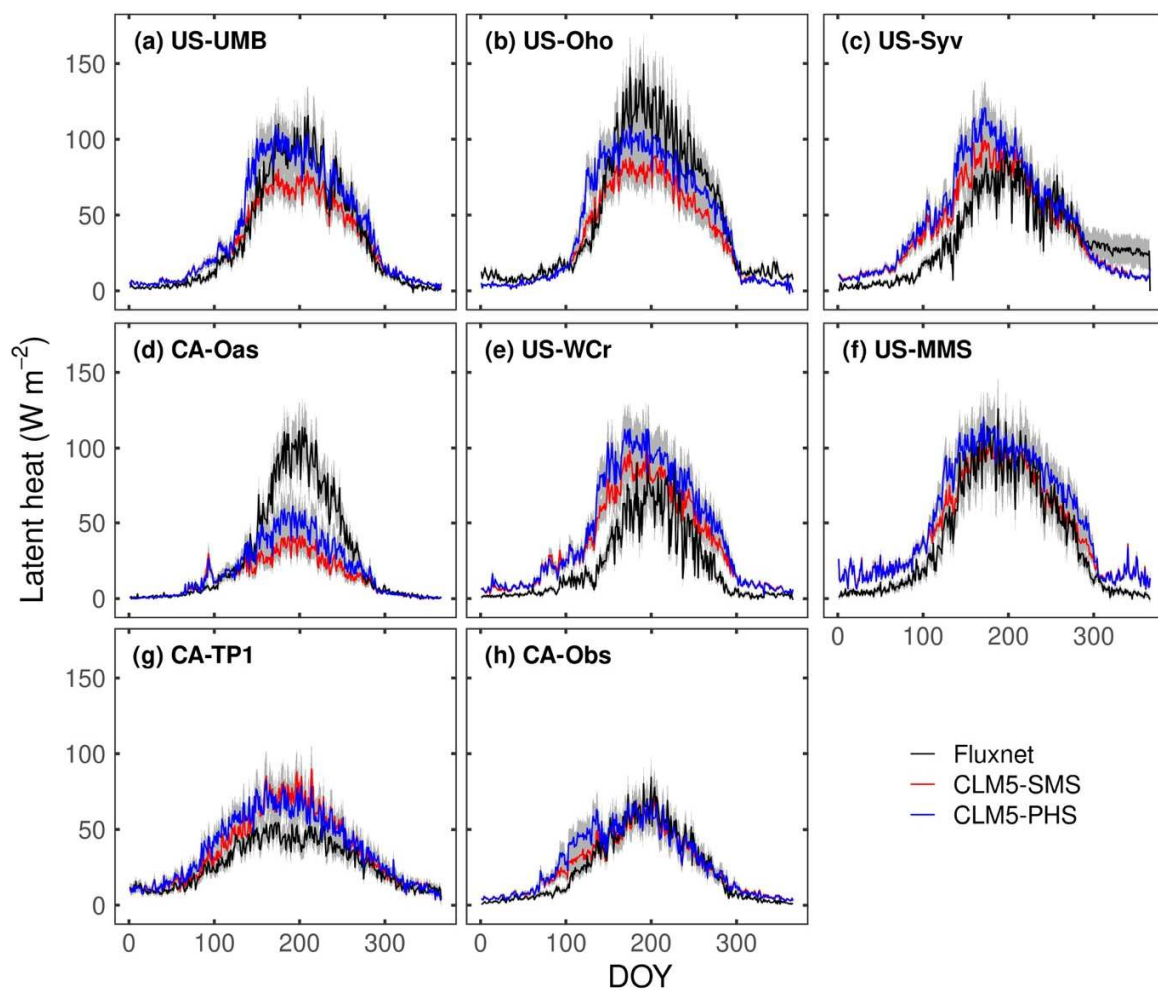
**Figure 5.** Mean annual (2004-2010) seasonal cycle (lines) and 95% confidence intervals (gray envelopes) for observed Fluxnet and CLM5 simulated latent heat flux. Sites are ordered from dry to wet, and arranged as DBF (top and center rows) and ENF (bottom row).
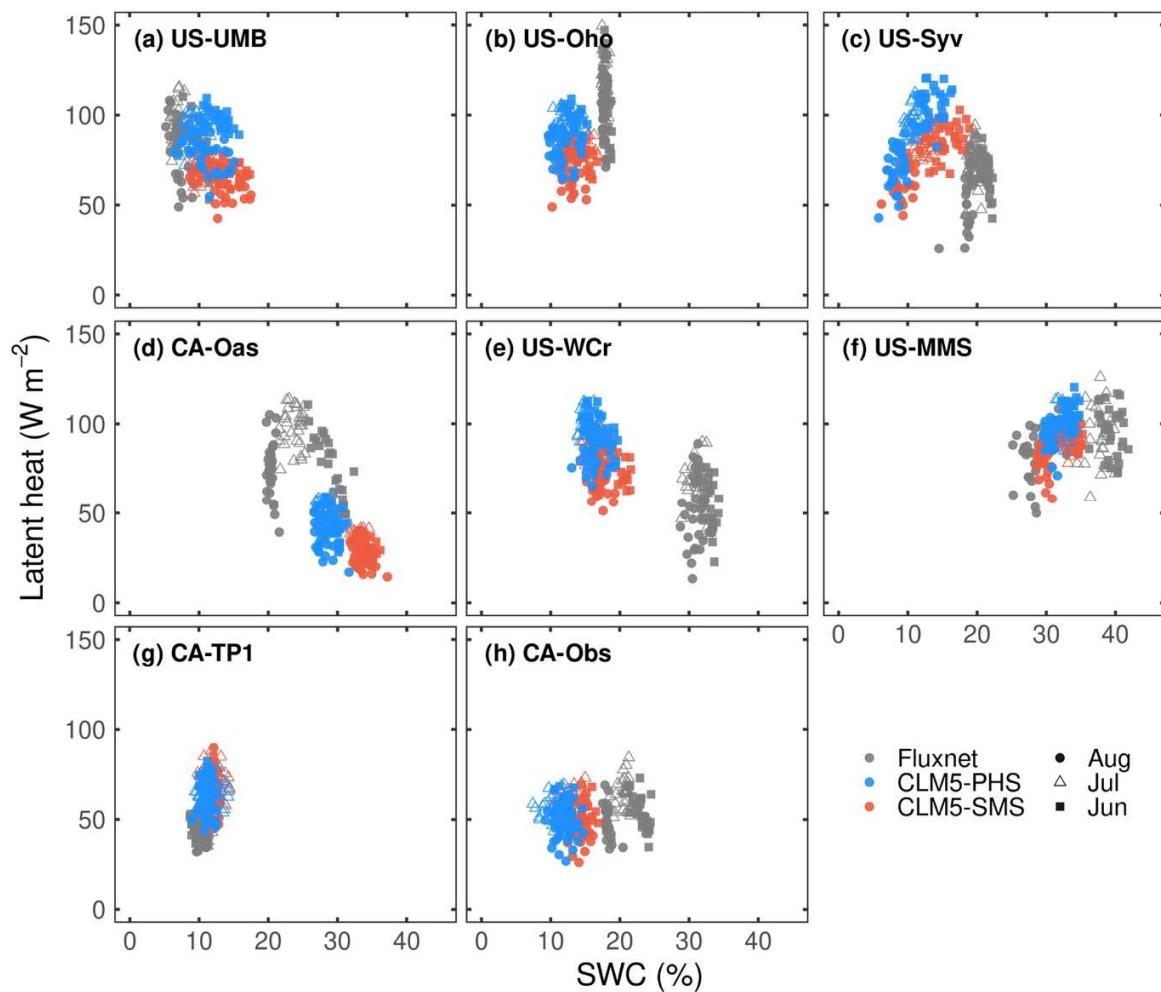
35

**Figure 6.** Observed (grey; Fluxnet) and simulated CLM5-PHS (blue) and CLM5-SMS (red) relationship between latent heat flux (W m$^{-2}$) and surface soil moisture (SWC). Data are based on daily climatologies for June (squares), July (triangles) and August (circles) from 2004-2010.
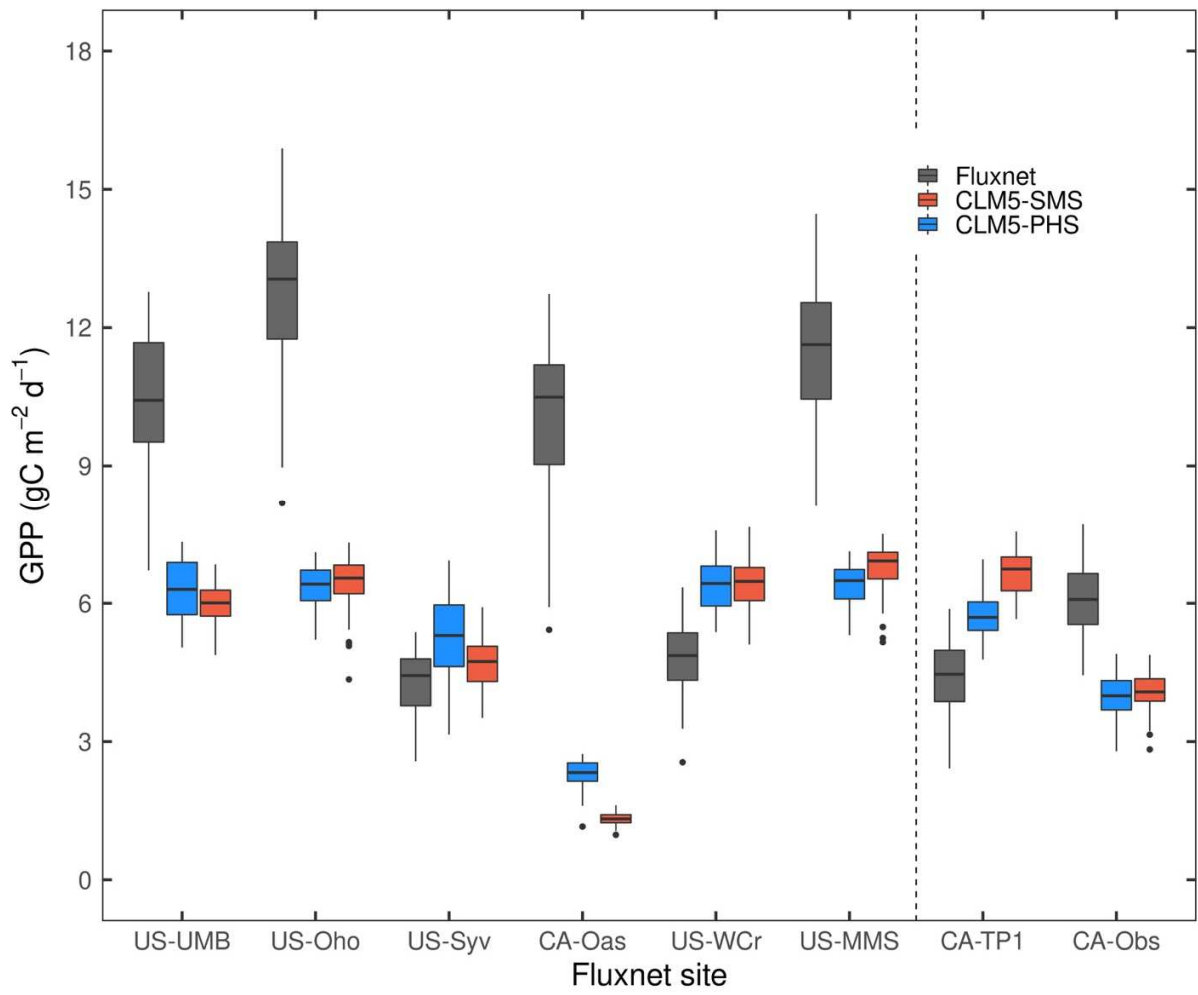
36

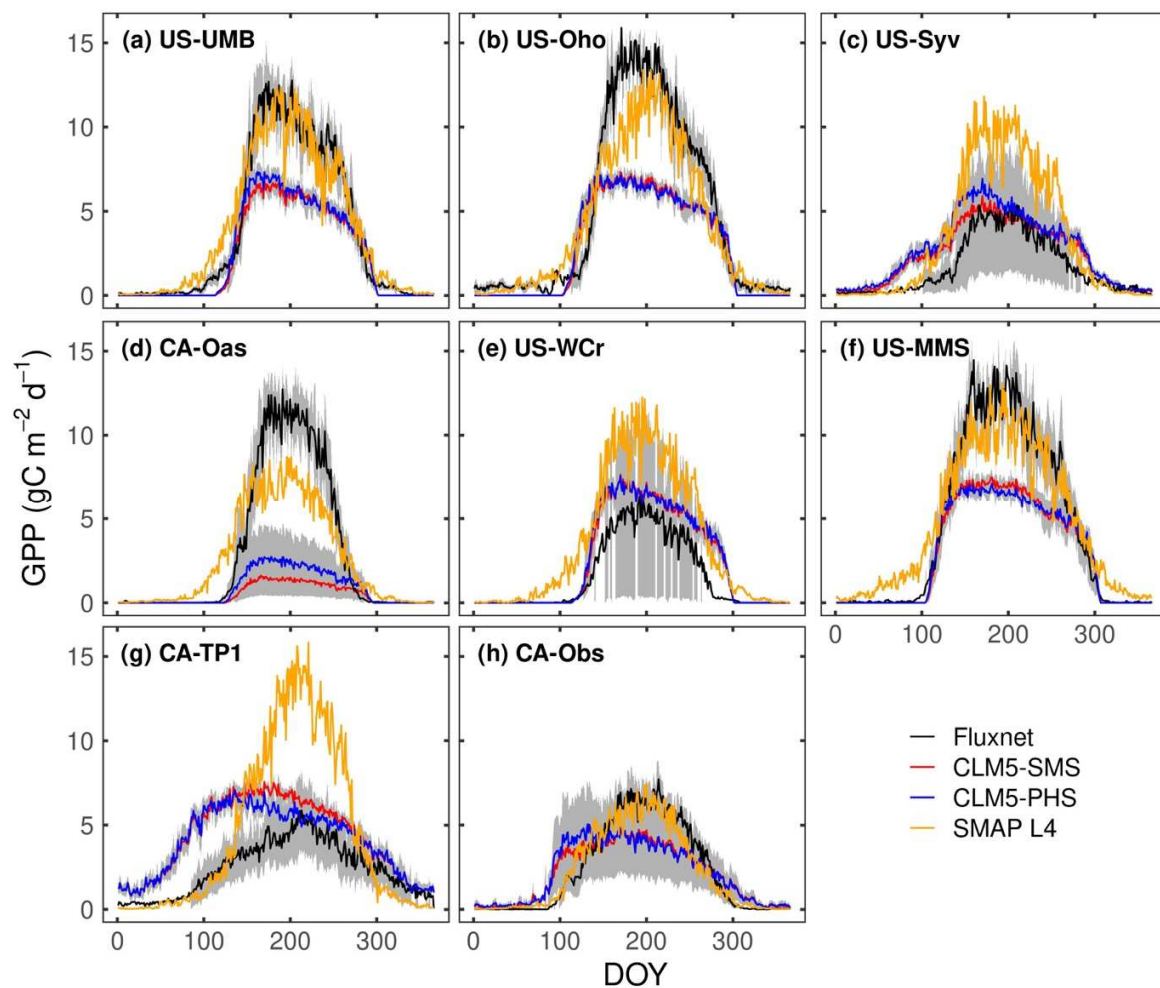**Figure 7.** Same as Figure 4, but for GPP.

**Figure 8.** Same as Figure 5, but for GPP. SMAP L4 climatological GPP (orange) is included for the time period April 2015-November 2018.
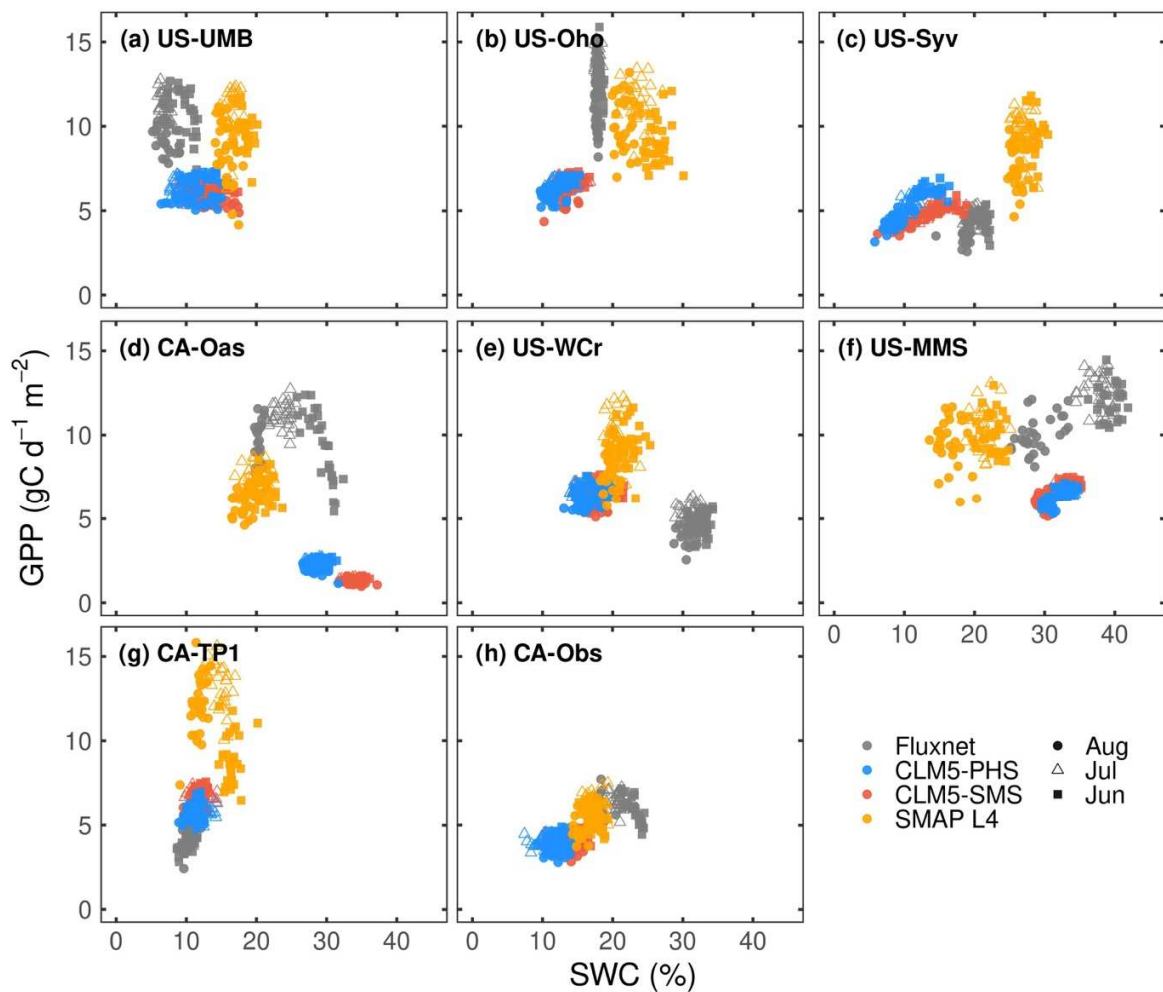
38

**Figure 9.** Same as Figure 6, but for GPP. SMAP Level 4 data (orange) is also included from April 2015-November 2018.
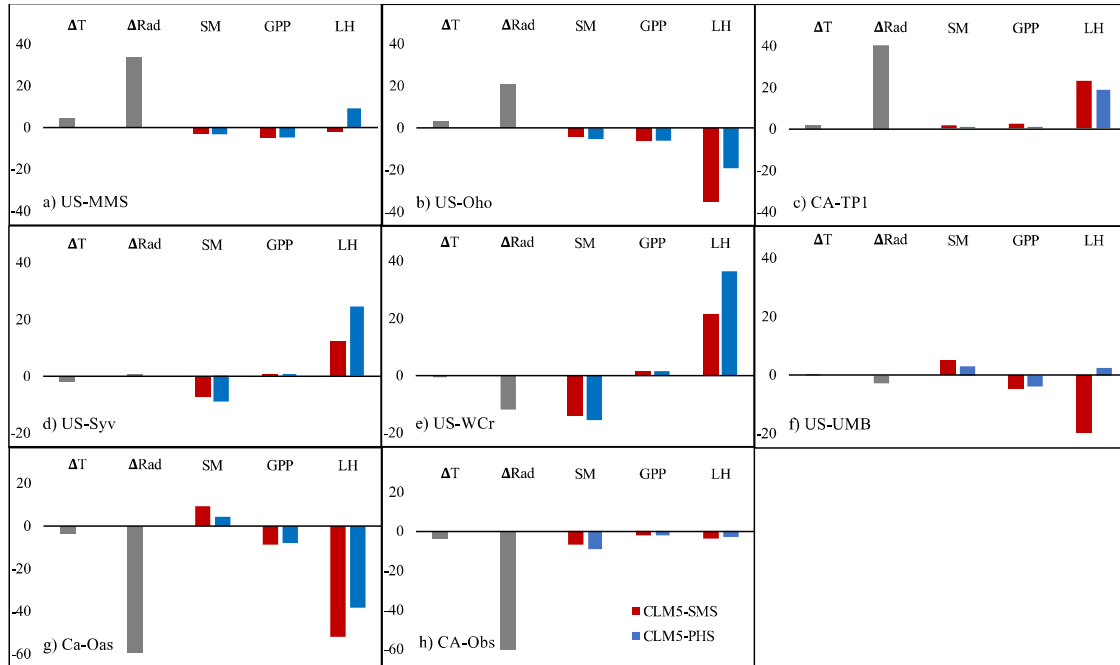
**Figure 10.** Summary of site climatological conditions and model biases. Site-to-site differences in annual average temperature ($\Delta T$;K) and annual average incoming solar radiation ($\Delta R$; W m$^{-2}$) represent the variability in site conditions from the observed mean of 8 Fluxnet sites, indicating sites that are relatively warmer or cooler or receive more or less radiation. Site biases for JJA mean latent heat (W m$^{-2}$) and GPP (g C m$^{-2}$ d$^{-1}$) are presented as the difference between CLM and Fluxnet observations at individual sites.

40

Latent heat (W m$^{-2}$)

(a) US-UMB
(b) US-Oho
(c) US-Syv
(d) CA-Oas
(e) US-WCr
(f) US-MMS
(g) CA-TP1
(h) CA-Obs

Fluxnet
CLM5-SMS
CLM5-PHS

DOY

Figure with 8 panels (a)–(h) showing GPP (gC m⁻² d⁻¹) versus DOY for different sites.

Y-axis label: GPP (gC m$^{-2}$ d$^{-1}$)

X-axis label: DOY

Panel labels:
(a) US-UMB
(b) US-Oho
(c) US-Syv
(d) CA-Oas
(e) US-WCr
(f) US-MMS
(g) CA-TP1
(h) CA-Obs

Legend:
Fluxnet
CLM5-SMS
CLM5-PHS
SMAP L4

a) US-MMS

b) US-Oho

c) CA-TP1

d) US-Syv

e) US-WCr

f) US-UMB

g) Ca-Oas

h) CA-Obs

CLM5-SMS
CLM5-PHS